Electrocatalytic Oxidation of Dinitrogen to Nitric Acid via Direct Ten–Electron Transfer Using Manganese Phthalocyanine

Ashadul Adalder[1], Sourav Paul[1], Biswajit Ghorai[1], Samadhan Kapse[2], Ranjit Thapa[2], Abharana N.,[3] and Uttam Kumar Ghorai[1, *]

[1]Department of Industrial Chemistry & Applied Chemistry, Swami Vivekananda Research Centre, Ramakrishna Mission Vidyamandira, Belur Math, Howrah, 711202, India

[2]Department of Physics, SRM University – AP, Amaravati, Andhra Pradesh, 522240, India

[3]Atomic & Molecular Physics Division, Bhabha Atomic Research Centre, Mumbai, 400085, India

Corresponding author:

*Email: uttam.indchem@vidyamandira.ac.in

ABSTRACT: Ammonia produced through the energy intensive Haber–Bosch process, undergoes catalytic oxidation for the manufacture of commercial nitric acid in the age–old Ostwald process. This two–step energetically non–viable industrial process demands the quest of an alternative single step electrocatalysis from the last century. The quest ends up in optimism when we unravel a ten–electron pathway associated with electrochemical dinitrogen oxidation reaction (N_2OR) to nitric acid by manganese phthalocyanine (MnPc) hierarchical nano–structures (HNs) at STP. The catalyst delivers nitric acid yield of 720 μmol h^{-1} g^{-1}_{cat} @ 1.9 V vs. RHE and F.E. of 17.32 % @ 1.7 V vs. RHE in 0.05 M HCl. The local co–ordination environment ($Mn–N_4$) during electrocatalysis process is ensured by the XAFS study. DFT based calculations express that the Mn site of MnPc is the main active center for nitrogen adsorption for N_2OR, suppressing the OER.

Introduction: Artificial nitrogen fixation utilizing chemical transformation technology of nitrogen based compounds, such as nitric acid (HNO_3), using green chemistry route is one of the prime demand of present time[1]. Nitric acid is a major key player in various industries and an extremely important chemical constituent of the nitrate based fertilizers for plant growth, gun powder, and explosives[2]. Commercial nitric acid is prepared by the 120 year old Ostwald process where NH_3 gets oxidized in presence of catalyst at high temperature (400–600°C) and pressure (15–25 MPa). This process is extremely energy demanding and produces extravagant amount of greenhouse gases (CO_2) into the atmosphere[1].To produce NH_3 in the industrial scale, Haber–Bosch process is employed where raw materials (N_2 & H_2) are treated at high temperature (700K) and pressure (150 atm). This process consumes 1% of the total global energy and produces 1.9 metric ton of greenhouse gas (CO_2) per metric ton of NH_3 synthesis [1, 3]. Therefore, the deletion of the dual step HNO_3 synthesis method forms a mandatory requirement to address the issue and provide an alternate sustainable solution yet catering to the demand of the market. Electrocatalytic dinitrogen oxidation reaction (N_2OR) using electrocatalyst under ambient conditions is an optimistically promising alternative to develop sustainable nitrate product using various heterogeneous catalysts such as Ru/TiO_2, Pd–MXene, $ZnFe_xCo_{2-x}O_4$, Fe–SnO_2, Nb_2O_{5-x}, Pd-s PNSs, etc. [4-14]. Electrocatalytic N_2 oxidation processes follow a two–step pathway. In the first step, N_2 reacts with *O to form NO* intermediate and followed by the reaction of NO* with H_2O and O* to form the nitrates [12]. Simultaneously, competing four electron oxygen evaluation reaction (OER) takes place in the first stage which is the rate limiting step. From the partial Pourbaix diagram for N_2–H_2O system, it is noted that N_2OR is more favorable for nitrate

synthesis over OER while pH is greater than 1.3 [1, 16]. Thus, strategic design with precise selection of N_2OR electrocatalyst is extremely important to sufficiently suppress the OER and promote the N_2OR in the same potential window. Recently metal phthalocyanines (M=Co, Ni and Fe) have showcased as high performance NRR electrocatalyst for N_2 fixation to NH_3 owing to its metal centre based $M–N_4$ active sites [15-17]. In addition to that, manganese phthalocyanine (MnPc) also does structurally possess $Mn–N_4$ active sites [18], and its superiority for electrochemical N_2OR is yet to be unraveled by the scientific fraternity.

In this regard, Prof. Nørskov and co–workers [19] have developed a theoretical model to understand the probable reaction mechanisms at the molecular level of N_2 oxidation to direct HNO_3 via ten electron transfer process $[N_{2(g)} + 6H_2O_{(l)} \rightarrow 2HNO_{3(l)} + 10H^+ + 10e^-]$ with the reaction of N_2 and *OH. They have not only studied the reaction pathway but also have shown the clearer understanding of the competition reaction between OER and N_2OR on the oxide surface. Inspired by their theoretical research work on N_2OR, we have demonstrated MnPc HNs as N_2OR electrocatalyst to synthesize nitric acid, through the ten electron reaction pathways. The MnPc HNs delivers a nitric acid yield rate of 720 µmol h^{-1} g^{-1}_{cat} @ 1.9 V vs. RHE and F.E. of 17.32 % @ 1.7 V vs. RHE in 0.05 M HCl. The nitric acid yield was quantitatively estimated by ion chromatographic method. Isotopic labeling experiment has been further carried out to decipher the actual source of nitrogen in nitric acid by the ^{15}N–nuclear magnetic resonance (^{15}N–NMR). DFT computations substantiate the above study with identifying the prime active centers for N_2 adsorption in MnPc. We have further confirmed that the N_2OR is a dominant reaction over OER in the same potential on both Mn and C sites in MnPc catalyst.

Results and discussion

Theory guided catalyst design for N₂OR: The reaction mechanism, overpotential and active sites of electrochemical N_2 oxidation reaction (N_2OR) are investigated by using density functional theory based method. Firstly, we demonstrate the complete free energy profile of ten electrons N_2OR [19] considering each intermediate on MnPc as shown in **Figure 1b**. The other possible pathways for N_2OR are shown in **Figure SI**. The pathways we considered are alternating (simultaneous oxidation of both N atoms) and distal (one by one N atom oxidation) at applied potential U = 0 V. Also, it is reported that the oxidation of first nitrogen can be via Langmuir–Hinshelwood (LH) or Eley–Rideal (ER) mechanism [8, 19]. In the LH mechanism, the OH^- ion is captured by electron deficient Carbon (C) site adjacent to the Mn site with N_2 pre–adsorbed on the Mn site (formed *N_2*OH), following the formation of *NNO or *N_2*O in the next step. After the mentioned step, alternate or distal pathway(s) are followed. In ER mechanism, the OH^- ion directly attached with the pre–adsorbed N_2 to form *NNOH. We found that the LH mechanism is more promising than ER for the first oxidation of N_2 by 1.05 eV energy (step 2 in the **Figure SI**). Further, the alternate pathway is preferred over distal due to 0.48 eV lower in free energy steps (step 4 in **Figure SI**). As shown in **Figure 1b**, the full free energy profile of N_2OR at applied potential U = 0 V, equilibrium potential (1.15 V) and the limiting potential (1.77 V). At limiting potential U = 1.77 V, all the steps in free energy profile becomes downhill and exothermic for preparation of nitric acid. At the equilibrium potential (U = 1.15 V), the reactants and products are at equilibrium and the highest uphill step in free energy is a potential determining step, which is used to define thermodynamic overpotential (η) (limiting potential – equilibrium potential) for N_2OR. Recently, the TiO_2 catalyst are theoretically investigated for N_2OR, which shows η = 2.08 V [19]. Similarly, for MnPc catalyst, we

have confirmed the first step protonation, *NNO to *NONOH as the potential determining step and the overpotential (η) is only 0.62 V. It is to be noted that, the final step *NO₃H to free HNO₃, which involves the release of nitric acid without a proton/electron transfer does not belong to the N₂OR.
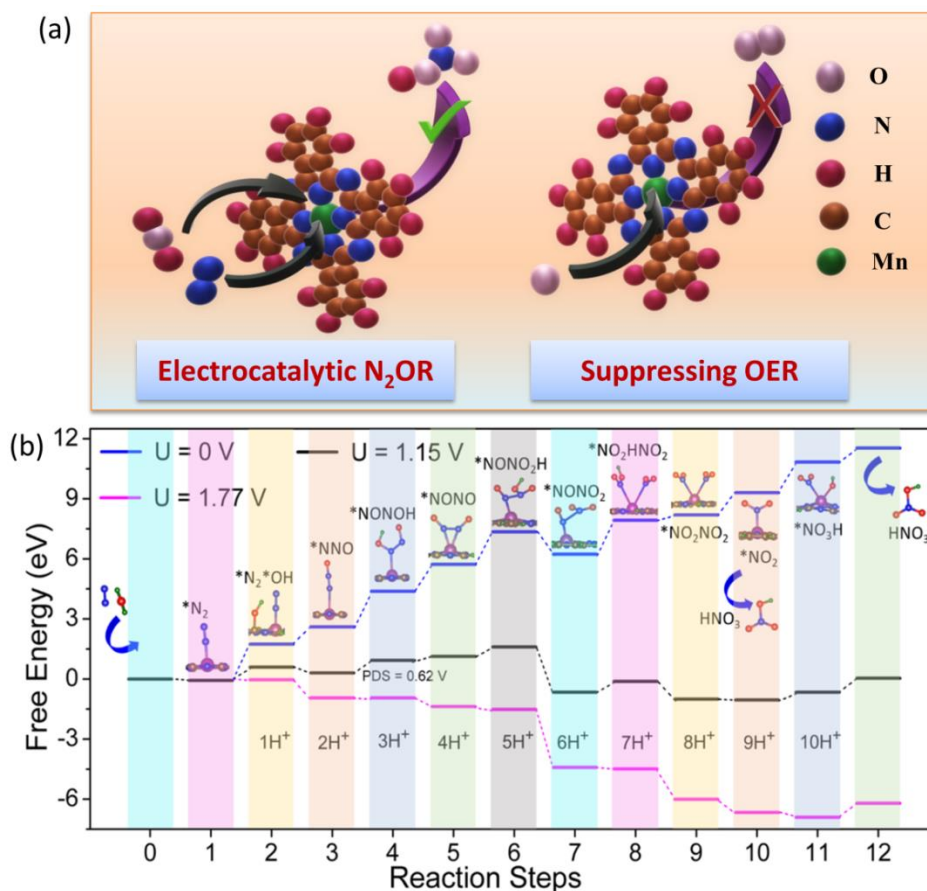

Figure 1: *a) Schematic representation of nitric acid synthesis process on the surface of MnPc; b) Demonstrate the free energy profile of ten electron electrochemical N₂ oxidation reaction on MnPc catalyst at applied potential U= 0 V, 1.15 V (equilibrium potential), 1.77 V (limiting potential). Here PDS indicate the potential determining step. Dotted lines are to guide the eye.*

Electrocatalyst synthesis and its characterization: The MnPc HNs were prepared by solvothermal method, where phthalonitrile and manganese acetate are used as reactants with ethylene glycol as solvent medium. The detailed reaction mechanism is demonstrated in the

Figure 2a. In this reaction, ethylene glycol acts as a nucleophile and it makes an attack to the cyano group present in phthalonitrile molecules. An intermediate product is produced in the reaction which further combines together to form a stable MnPc molecule. To determine the crystal structure and phase purity of MnPc crystal, X–ray diffraction technique (XRD) was used. The XRD pattern (**Figure 2b**) are well matched with the standard ICDD card no #02–063–3894 of MnPc with present space group of $P2_{1/c}$ [20]. The first two peaks at 6.90° and 9.11° confirms the formation of β–MnPc structure. All intense XRD planes are indexed as (100), ($\bar{1}$02), (002), ($\bar{2}$02), ($\bar{3}$02), and ($\bar{1}$04) at the 2θ theta values of 6.90°, 9.11°, 10.49°, 12.50°, 18.1°, and 18.52°.
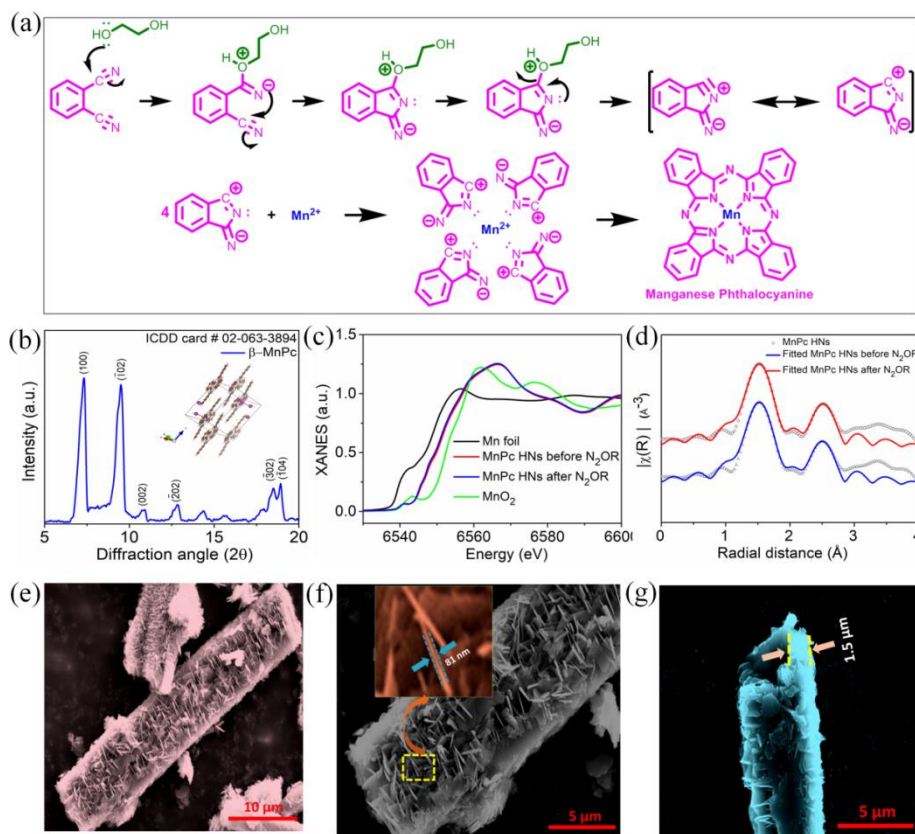

Figure 2:*(a) Reaction mechanism for the synthesis of MnPc molecule (b) XRD pattern of MnPc HNs; (c) Normalized XANES spectra at the Mn K–edge; (d) Experimental χ(R) vs R data of MnPc HNs measured at the Mn K–edge with fitting; (e), (f) & (g) FESEM images of MnPc HNs at different magnifications.*

Fourier transformed infrared spectroscopy (FTIR) technique was performed to examine the chemical bonds present in the MnPc crystal (**Figure SI**). To study the different type of chemical composition present in MnPc crystal, X–ray photoelectron spectroscopy (XPS) technique was performed. The survey scan (**Figure SI**) proves the presence of Mn, C and N atoms in MnPc crystal. The high resolution spectrum of N1s in the XPS spectrum shows the two peaks (**Figure SI**) at 399.33 eV and 400.42 eV resulting to the pyridinic–N and pyrrolic–N present in MnPc. In MnPc, pyridinic nitrogen atoms are attached with carbon atoms and pyrrolic nitrogen atoms are bonded with Mn–metal center. Synchrotron based X–ray absorption near–edge structure (XANES) was performed to study the electronic configuration of manganese in MnPc electrocatalyst before and after N_2OR process. **Figure 2c** shows the normalized XANES spectra of MnPc HNs before and after N_2OR electrolysis measured at Mn K–edge along with that of the metal foil and MnO_2 standard. It has been observed that the X–ray absorption edge position of MnPc lies in between Mn foil and MnO_2 and hence the oxidation state of 'Mn' in MnPc lies between 0 and +4 [21, 22]. To study the local coordination environment of the Mn in MnPc electrocatalyst, extended X–ray absorption fine structure (EXAFS) analysis was carried at +1.9 V vs. RHE before and after N_2OR electrolysis. **Figure 2d** shows the Fourier–transformed (FT)–EXAFS spectra of the MnPc HNs samples (before and after electrolysis) exhibiting an intense peak at 1.5 Å which can be assigned to the first shell Mn–N co–ordination bonds [23]. From the quantitative fitting of Fourier transformed k^2 weighted EXAFS (FT–EXAFS) spectra, the obtained co–ordination number of Mn with surrounding nitrogen is four which is almost same during N_2OR process and prior to it (**Figure 2d and Table SI**). The FESEM images of MnPc hierarchical nanostructure with different magnifications is shown in **Figure 2e–g**. In **Figure 2e**, the microstructure of the MnPc shows a quadrangular shape with average length and

diameter of ~50 μm and ~5 μm. Furthermore, the detailed microstructure of the MnPc HNs at higher magnification is shown in the **Figure 2f**, which demonstrates that the micro quadrangular shapes were made by the densely packed nanoflakes. The thickness of the nanoflakes is in the range of ~75 to ~100 nm. The hollow interior space in the HNs is clearly observed in the **Figure 2g**.

Electrocatalytic N_2OR performance towards nitric acid synthesis: The evaluation of the electrochemical nitric acid synthesis performance was executed in a three electrode setup utilizing chronoamperometry method at constant potentials. The subjected electrolyte (0.05 M HCl) was saturated by effervescing nitrogen or argon gas of ultra-high pure grade. (**Figure SI** and details explanation in electrochemical set–up).
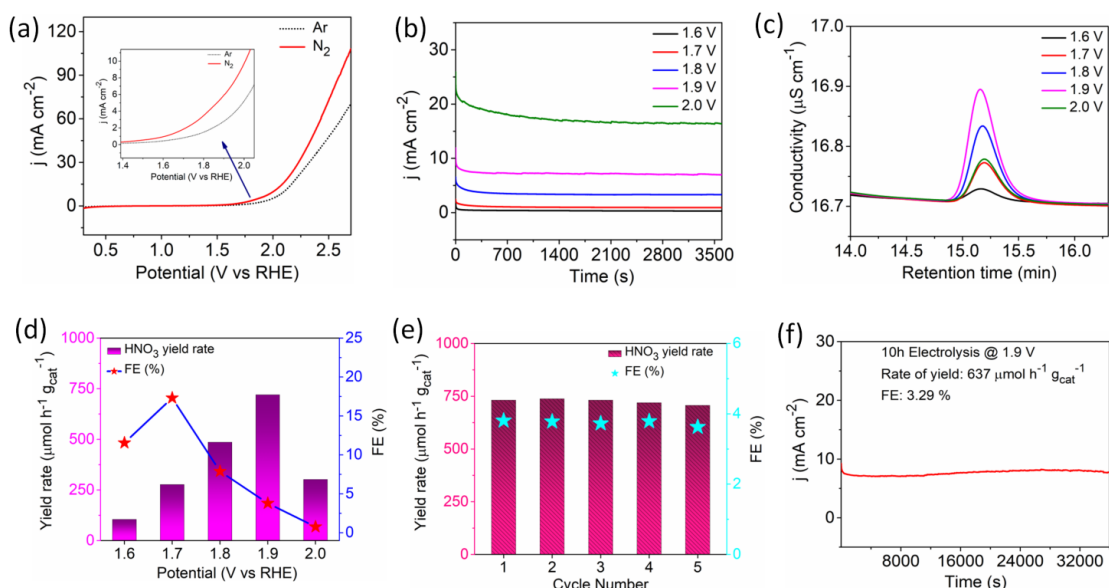

Figure 3: (a) LSV profile of MnPc HNs in Ar & N_2 saturated 0.05 M HCl solution; (b) Time reliant current density (j) curves for MnPc HNs at various potential; (c) Ion chromatogram spectra of the electrolytes at different potential after 3600 sec N_2OR electrolysis; (d) Bar chart of average HNO_3 yield rate and corresponding Faradaic efficiency of MnPc HNs at different potential; (e) Recycling stability tests of MnPc HNs for N_2OR at 1.9 V vs. RHE for five times; (f) 10 h durability test for MnPc HNs towards N_2OR at 1.9V vs. RHE in N_2 saturated electrolyte

8

The electrocatalyst mass were loaded and optimized condition were achieved to precisely determine the faradic efficiency. Linear sweep voltammetry (LSV) was used to initially evaluate the electrocatalytic performance of MnPc HNs. As shown in **Figure 3a**, the MnPc HNs demonstrates an augmentation in current density in N_2 saturated 0.05 M HCl compared to the Ar saturated electrolyte, implying the formation of electrochemical nitric acid. The electrocatalysis tests are executed at the potentials of 1.6 to 2.0 V vs. RHE, the ion chromatograph and chronoamperometry results are exhibited in **Figure 3b and 3c.** The peak area attains the maxima at 1.9 V vs. RHE where the nitric acid yield is 720 µmol h^{-1} g^{-1}_{cat} shown in **Figure 3d.** It is to be noted that at the same potential, nitric acid faradic efficiency is 3.8%, however the dramatically elevated faradic performance of 17.32 % were observed at 1.7 V vs. RHE. The yield rate of nitric acid almost linearly increases from the potential of 1.6 to 1.9 V vs RHE., beyond the positive potential, the electrochemical nitric acid synthesis performance drops down due to the enhancement of the competing OER at the higher potential than the N_2OR in the electrode surface [15]. The sturdy electrochemical activity of MnPc HNs is displayed in the longstanding (10 h) chronoamperometry results in **Figure 3f.** This can be attributed to the retention of the structural integrity of the crystalline phase of the catalyst during the progress of electrochemical process, the corresponding UV–vis, XRD, and XPS study (**Figures SI**) of the MnPc HNs confirms the chemical and structural stability of the catalyst during N_2OR process.

The control experiment was carried out in 0.05 M HCl without any nitrogen source (argon gas was bubbled, open circuit condition) which resulted in negligible amount of nitric acid production as displayed in ion chromatogram (**Figure SI**). This clearly shows that the N element in HNO_3 actually emerges for the bubbled N_2 gas. To further decipher the source of nitrogen in nitric acid, isotope labelling electrochemical experiments was also carried out by

bubbling $^{15}N_2$ gas in the electrolyte. The characteristic singlet peak of ^{15}N labelled nitric acid where observed in the ^{15}N NMR spectrum at ~376 ppm (**Figure SI**) which validates that the oxidation of $^{15}N_2$ feed gas is solely responsible HNO_3 production [11]. The UV–vis absorption spectra of the standard NO_2^- solution and N_2OR derived electrolytes at different potential confirm the absence of the NO_2^- as a by–product during electrocatalytic process as displayed in From **Figure SIa–SIb.** The primary indicators of industrial application of an electrocatalyst depends broadly on two parameters these are performance repeatability and process stability, as shown in **Figure 3e,** the MnPc HNs catalyst is relatively stable with consistent performance for five repeat cycle of electrochemical nitric acid production.

From the critical stand point, it is vital to understand the oxygen evolution reaction (OER), a parallel reaction occurring during N_2OR process [24], which compete and hinders the efficiency of N_2OR. Therefore, we have studied the possibility of OER on MnPc catalyst using free energy profile (**Figure SI**). Firstly, we observed that the OH adsorption on Mn site of MnPc (the first intermediate step for OER) [25] is endothermic with free energy change (+0.605 eV), whereas N_2 adsorption is favorable with exothermic free energy change of -0.069 eV. Secondly, we have pinpointed the preferred mechanism to be LH, further estimations reveal whether the adsorbed OH on C site can lead to OER or not. It is observed that the free energies of *N_2*O and *N_2*OOH steps of OER are higher than the *NNO and *NONOH steps of N_2OR respectively. However, both *OH or *O on C site can react with *N_2 to form *NNO, which helps in N_2OR pathways by suppressing OER on C site. Also, we have computed the limiting potential (U = 2.38 V) for OER (**Figure SI**) on Mn site which is very high compared to the limiting potential (U = 1.77 V) for N_2OR process. Therefore, we hereby confirm that the N_2OR is a dominant reaction over OER on both Mn and C sites of MnPc catalyst. Further, we have studied the

adsorption behavior of N_2 on different possible active sites of MnPc as shown in **Figure 4a**. The free energy change for adsorbed N_2 on different sites is obtained in the following order: Mn (-0.069 eV) > pyridinic–N1 (-0.038 eV) > pyrrolic–N2 (-0.023 eV) > pyrrolic–N3 (-0.017 eV) > Carbon (-0.002 eV). It epitomizes the Mn site of MnPc to play the role of prominent active site for N_2 adsorption. The molecular adsorption behavior of Mn site is correlated with d band center of Mn atom [26] (**Figure 4b-d**).
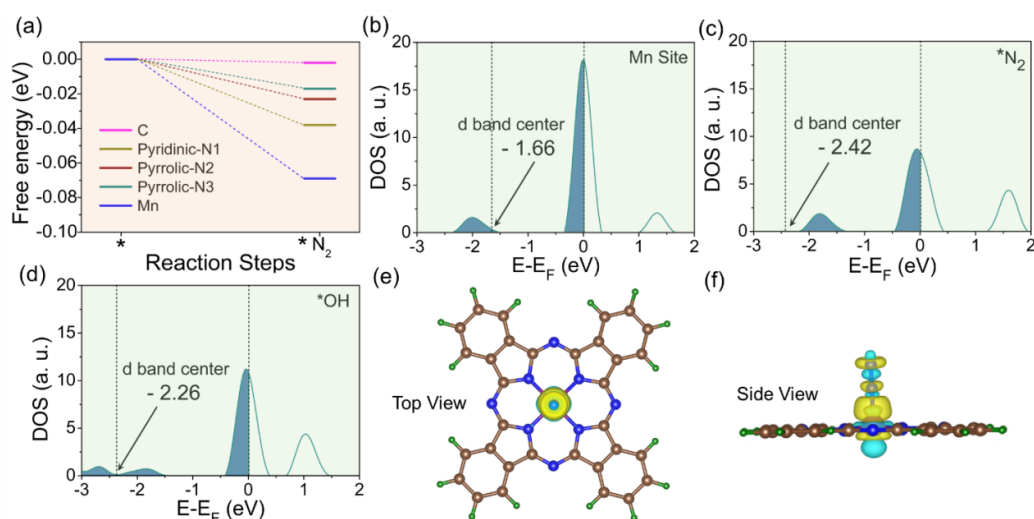

Figure 4 *(a) Free energy of N_2 adsorption on possible active sites of MnPc. The projected density of states of d orbital for (b) Mn site (c) Mn site after N_2 adsorption (d) Mn site after OH adsorption. The charge density difference of MnPc after N_2 adsorption (e) Top view (f) Side view. The Mn, N, O, C, H atoms are denoted with pink, blue, red, wine, and green color sphere respectively. Yellow and blue lobes indicate electron accumulation and depletion, respectively (Isosurface value = 0.005 e/A³).*

The calculated d-band center of Mn atom of MnPc is at -1.66 eV, and after adsorption of N_2 and OH molecules, it is found that the d band center shifted towards the negative energy and obtained at -2.42 eV and -2.26 eV respectively. The higher shift in the d band center is the reason of exothermic free energy step of N_2 adsorption as compared to the endothermic step for OH

adsorption on Mn site. It indicates that the required charge transfer occurs from Mn site to adsorbed N_2, which is further visualized through charge density difference analysis (**Figure 4e-f**).

Conclusion: In summary, we have developed a strategy towards direct ten–electron oxidation of dinitrogen to nitric acid by MnPc HNs electrocatalyst under ambient conditions. The excellent N_2OR performances are achieved due to the specific–selectivity, presence of excess number of active sites, repeatability and longstanding sturdy nature of the electrocatalyst. Isotopic labelling experiment has been performed with ^{15}N nuclear magnetic resonance (NMR) to prove that the purged nitrogen gas is the sole source of N element in HNO_3. The X–ray absorption fine structures (XAFS) confirm that Mn atoms are coordinated to the pyrrolic and pyridinic N via Mn–N_4 coordination. Density functional theory (DFT) calculations reveal that the Mn site of MnPc is the prominent active site for N_2 adsorption and N_2OR is a dominant reaction over OER on both Mn & C sites of MnPc catalyst. This research work capitalizes on a new arena of N_2OR process leading to successful single step nitric acid synthesis using MnPc catalyst via ten electron transfer for the development to attain the near future global goal to make a carbon–neutral sustainable society.

Experimental Section

Materials: All commercially available chemicals were used any additional washing. Phthalonitrile (Sigma–Aldrich), ethylene glycol (Merck), ammonium heptamolybdate tetrahydrate (Merck), manganese acetate (Sigma–Aldrich), and HCl (Merck).

Synthesis method: MnPc HNs was prepared by solvothermal process. For the solvothermal method, a precursor solution was prepared by mixing of 1.8 mmol of phthalonitrile, 20 mg of ammonium hepta molybdate tetrahydrate, 0.45 mmol of manganese acetate and 72 ml of ethylene glycol solvent. Then, stir the mixture for 10–15 minutes and stop stirring when nucleation just start and transfer the solution mixture to an 100 ml autoclave Teflon cup. The temperature of the oven was kept at 180 ^{0}C for 22 hours. After the oven cooling, the solution was filtered with using Whatman 41 filter paper. The residue was washed several times with ethanol, 0.1 M HCl and hot water. Then, the precipitate was dried at 65 ^{0}C for 12h. Finally, MnPc sample was collected for further used.

Characterization techniques: X–ray diffraction technique (XRD) was used to observe the crystal structure and phase purity of synthesized MnPc. XRD analysis of MnPc was done utilizing the Bruker D–8 with advanced Eco X-ray powder diffractometer where the Cu–K$_\alpha$ was used as a monochromatic radiation with a wavelength value of 0.15404 nm. X-ray tube voltage and current condition were maintained at 40 kV and 25 mA, respectively. X–ray photoelectron spectroscopy (XPS) study of MnPc was done utilizing an OMICRON–0571 framework. FTIR analysis (Shimadzu IRAffinity-1S) was done to see the different type of chemical bond present in MnPc nanostructures. The morphological observation of synthesis MnPc was done by using the field emission scanning electron microscope (FESEM) (Thermo Scientific, Apreo–S). All electrochemical nitrogen oxidation analysis was done by CHI 760E instrument.

Electrochemical set–up: All electrochemical nitrogen oxidation processes were done in 0.05 M HCl solution with purging of ultra high pure nitrogen gas (N$_2$) (99.999 %) gas. Three electrodes setup was used for the nitrogen oxidation reaction (N$_2$OR) process where the catalyst loaded on carbon paper as working electrode, saturated Ag/AgCl was used as the reference electrode and

13

the counter electrode was platinum wire. Before starting any experiment, nitrogen gas was purged for 30 minutes to saturate in the electrolyte solution. All applied potential values were converted to the reversible hydrogen electrode (RHE).

Author information

Corresponding author:

*Email: uttam.indchem@vidyamandira.ac.in

FAX: 2654-1123; Phone: 91 33 26549181

ORCID

Uttam Kumar Ghorai: 0000-0003-0537-598X

Notes: UKG, AA and SP have filed an Indian Patent application (202131029797) regarding the electrochemical synthesis of nitric acid under ambient conditions. The remaining authors declare no competing interests.

AUTHOR CONTRIBUTIONS

UKG conceived the idea and designed the experiments. BG and AA synthesized the catalyst and performed the XRD, FTIR, UV-vis. AA and SP carried out all the electrochemical measurements and analyzed the results. SK and RT performed the theoretical (DFT) calculations. RT, SK, AA and SP analyzed the DFT results. AA and UKG wrote the original manuscript. All authors contributed to write the final version of the manuscript. UKG supervised the project.

References:

1.   Chen, J. G. *et al.* Beyond fossil fuel–driven nitrogen transformations. *Science (80-.).* **360**, (2018).

2.   Liu, Y. *et al.* Pothole-rich ultrathin WO_3 nanosheets that trigger N≡N bond activation of nitrogen for direct nitrate photosynthesis. *Angew. Chemie - Int. Ed.* **58**, 731–735 (2019).

3.   Brown, K. A. *et al.* Light-driven dinitrogen reduction catalyzed by a CdS:nitrogenase MoFe protein biohybrid. *Science (80-.).* **352**, 448–450 (2016).

4.   Wang, Y., Li, T., Yu, Y. & Zhang, B. Electrochemical synthesis of nitric acid from nitrogen oxidation. *Angew. Chemie Int. Ed.* (2021) doi:10.1002/anie.202115409.

5.   Li, T. *et al.* Ru-doped Pd nanoparticles for nitrogen electrooxidation to nitrate. *ACS Catal.*

14032–14037 (2021) doi:10.1021/acscatal.1c04360.

6.   Wang, Y., Yu, Y., Jia, R., Zhang, C. & Zhang, B. Electrochemical synthesis of nitric acid from air and ammonia through waste utilization. *Natl. Sci. Rev.* **6**, 730–738 (2019).

7.   Zhang, L. *et al.* A janus Fe-SnO$_2$ catalyst that enables bifunctional electrochemical nitrogen fixation. *Angew. Chemie - Int. Ed.* **59**, 10888–10893 (2020).

8.   Dai, C., Sun, Y., Chen, G., Fisher, A. C. & Xu, Z. J. Electrochemical oxidation of nitrogen towards direct nitrate production on spinel oxides. *Angew. Chemie - Int. Ed.* **59**, 9418–9422 (2020).

9.   Han, S., Wang, C., Wang, Y., Yu, Y. & Zhang, B. Electrosynthesis of nitrate via the oxidation of nitrogen on tensile-strained palladium porous nanosheets. *Angew. Chemie - Int. Ed.* **60**, 4474–4478 (2021).

10.   Zhang, Y. *et al.* Electrocatalytic fixation of N$_2$ into NO$_3^-$: Electron transfer between oxygen vacancies and loaded Au in Nb$_2$O$_5^-$: Xnanobelts to promote ambient nitrogen oxidation. *J. Mater. Chem. A* **9**, 17442–17450 (2021).

11.   Fang, W. *et al.* Boosting efficient ambient nitrogen oxidation by a well-dispersed Pd on MXene electrocatalyst. *Chem. Commun.* **56**, 5779–5782 (2020).

12.   Kuang, M. *et al.* Efficient nitrate synthesis via ambient nitrogen oxidation with Ru-doped TiO$_2$/RuO$_2$ electrocatalysts. *Adv. Mater.* **32**, 1–7 (2020).

13.   Lan, J. *et al.* Nanoporous B$_{13}$C$_2$ towards highly efficient electrochemical nitrogen fixation. *Small* **17**, 1–7 (2021).

14.   Guo, Y. *et al.* Electrochemical nitrate production via nitrogen oxidation with atomically

dispersed Fe on N-doped carbon nanosheets . *ACS Nano* (2021) doi:10.1021/acsnano.1c08109.

15.   Ghorai, U. *et al.* Scalable production of cobalt phthalocyanine nanotubes: efficient and robust hollow electrocatalyst for ammonia synthesis at room temperature. *ACS Nano* **15**, 5230–5239.

16.   Murmu, S. *et al.* Unveiling the genesis of the high catalytic activity in nickel phthalocyanine for electrochemical ammonia synthesis. *J. Mater. Chem. A* **9**, 14477–14484 (2021).

17.   He, C. *et al.* Identification of FeN_4 as an efficient active site for electrochemical N_2 reduction. *ACS Catal.* **9**, 7311–7317 (2019).

18.   Mukherjee, M., Samanta, M., Banerjee, P., Chattopadhyay, K. K. & Das, G. P. Endorsement of manganese phthalocyanine microstructures as electrocatalyst in ORR: Experimental and computational study. *Electrochim. Acta* **296**, 528–534 (2019).

19.   Anand, M., Abraham, C. S. & Nørskov, J. K. Electrochemical oxidation of molecular nitrogen to nitric acid-towards a molecular level understanding of the challenges. *Chem. Sci.* **12**, 6442–6448 (2021).

20.   Wang, Z. & Seehra, M. S. Ising-like chain magnetism, arrhenius magnetic relaxation, and case against 3D magnetic ordering in β-manganese phthalocyanine (C32H16MnN8). *J. Phys. Condens. Matter* **28**, (2016).

21.   Di Castro, V. & Polzonetti, G. XPS study of MnO oxidation. *J. Electron Spectros. Relat. Phenomena* **48**, 117–123 (1989).

22. Chen, M. *et al.* Atomically dispersed MnN_4 catalysts via environmentally benign aqueous synthesis for oxygen reduction: mechanistic understanding of activity and stability improvements. *ACS Catal.* **10**, 10523–10534 (2020).

23. Li, J. *et al.* Atomically dispersed manganese catalysts for oxygen reduction in proton-exchange membrane fuel cells. *Nat. Catal.* **1**, 935–945 (2018).

24. Man, I. C. *et al.* Universality in oxygen evolution electrocatalysis on oxide surfaces. *ChemCatChem* **3**, 1159–1165 (2011).

25. Kapse, S., Janwari, S., Waghmare, U. V. & Thapa, R. Energy parameter and electronic descriptor for carbon based catalyst predicted using QM/ML. *Appl. Catal. B Environ.* **286**, 119866 (2021).

26. Hammer, B. & Nørskov, J. K. Theoretical surface science and catalysis—calculations and concepts. *Adv. Catal.* **45**, 71–129 (2000).